nature neuroscience

Intervening inhibition underlies simple-cell receptive field structure in visual cortex

Bao-hua Liu[1], Pingyang Li[1], Yujiao J Sun[1], Ya-tang Li[1], Li I Zhang[1,2] & Huizhong Whit Tao[1,3]

Synaptic inputs underlying spike receptive fields are important for understanding mechanisms of neuronal processing. Using whole-cell voltage-clamp recordings from neurons in mouse primary visual cortex, we examined the spatial patterns of their excitatory and inhibitory synaptic inputs evoked by On and Off stimuli. Neurons with either segregated or overlapped On/Off spike subfields had substantial overlaps between all the four synaptic subfields. The segregated receptive-field structures were generated by the integration of excitation and inhibition with a stereotypic 'overlap-but-mismatched' pattern: the peaks of excitatory On/Off subfields were separated and flanked colocalized peaks of inhibitory On/Off subfields. The small mismatch of excitation/inhibition led to an asymmetric inhibitory shaping of On/Off spatial tunings, resulting in a great enhancement of their distinctiveness. Thus, slightly separated On/Off excitation, together with intervening inhibition, can create simple-cell receptive-field structure and the dichotomy of receptive-field structures may arise from a fine-tuning of the spatial arrangement of synaptic inputs.

Simple and complex cells were first defined in the primary visual cortex (V1) of cats according to their distinctive spike receptive-field structures[1]. Simple-cell receptive fields are made up of spatially segregated On and Off subregions in which bright and dark stimuli, respectively, increase the cell's firing. In contrast, complex cells have overlapping On and Off subregions in their receptive fields[1,2]. A popular circuit model for simple-cell receptive fields, known as the push-pull circuit[3–7], proposes that the segregation of On and Off subfields results largely from the spatial arrangement of On- and Off-center excitatory inputs from thalamic relay cells and that the arrangement of inhibitory inputs is thought to be antagonistic to that of the excitatory thalamic inputs[5,6,8,9]. The push-pull model predicts that inhibitory and excitatory inputs evoked by the same contrast are largely segregated spatially and that inhibition does not contribute substantially to the segregation of the On and Off subfields. However, several experimental results contradict this model. First, an intracellular study in cats has suggested that the On and Off responses of simple cells may consist of both excitatory and inhibitory inputs[10]. Second, blocking GABA receptors extracellularly or intracellularly could convert simple-cell receptive fields to complex cell–like receptive fields[11,12]. These experimental data suggest that there may be a substantial spatial overlap between excitation and inhibition in simple cells and that inhibition may be crucial for generating the segregated On/Off receptive-field structure. More recently, it has been proposed that the spike threshold increases the difference in functional properties of simple and complex cells, which otherwise lie on a continuum if distributions of synaptic responses are considered[13–16]. This model implies that the push-pull circuit may only apply to the 'purest' simple cells.

To comprehend how specific receptive-field structures are generated, it is important to understand the distribution patterns of the underlying synaptic inputs. Most of the experimental evidence for the push-pull circuit comes from extracellular recordings of spike responses[17–20] or intracellular recordings of membrane potential responses[3,8,9,16,21]. These responses are the result of integrating excitatory and inhibitory synaptic inputs as well as voltage-dependent conductances, and may not be taken directly as either excitatory or inhibitory synaptic inputs. The synaptic circuit underlying simple-cell receptive fields requires further examination. Recent studies have shown that whole-cell voltage-clamp recordings can be reliably carried out in rodent cortices *in vivo*[22–26] and that the basic functional properties, such as simple/complex receptive-field structures and orientation and direction selectivity, are preserved in mouse V1 (refs. 27–31), making it a potentially good model for dissecting the synaptic input circuits underlying fundamental cortical processing of visual information. We used whole-cell voltage-clamp recordings to map four synaptic subfields for layer 2/3 neurons in the mouse V1: excitatory On and Off (Eon and Eoff) and inhibitory On and Off (Ion and Ioff) subfields. We found that the four synaptic subfields overlapped substantially in all of the neurons recorded. Spike receptive fields with segregated On and Off subfields were, in fact, generated from the synaptic integration of excitation and inhibition with a stereotypic spatial pattern, with the peaks of the Eon and Eoff segregated and those of the Ion and Ioff largely colocalized. Notably, the peaks of the Ion and Ioff were located between those of the Eon and Eoff. This configuration enables inhibition to exert an asymmetric shaping effect on the spatial tuning of On and Off responses, leading to a substantial enhancement of the spatial segregation between spike On and Off

[1]Zilkha Neurogenetic Institute, [2]Department of Physiology and Biophysics, [3]Department of Cell and Neurobiology, Keck School of Medicine, University of Southern California, Los Angeles, California, USA. Correspondence should be addressed to H.W.T. (htao@usc.edu) or L.I.Z. (liizhang@usc.edu).

Received 17 August; accepted 7 October; published online 29 November 2009; doi:10.1038/nn.2443

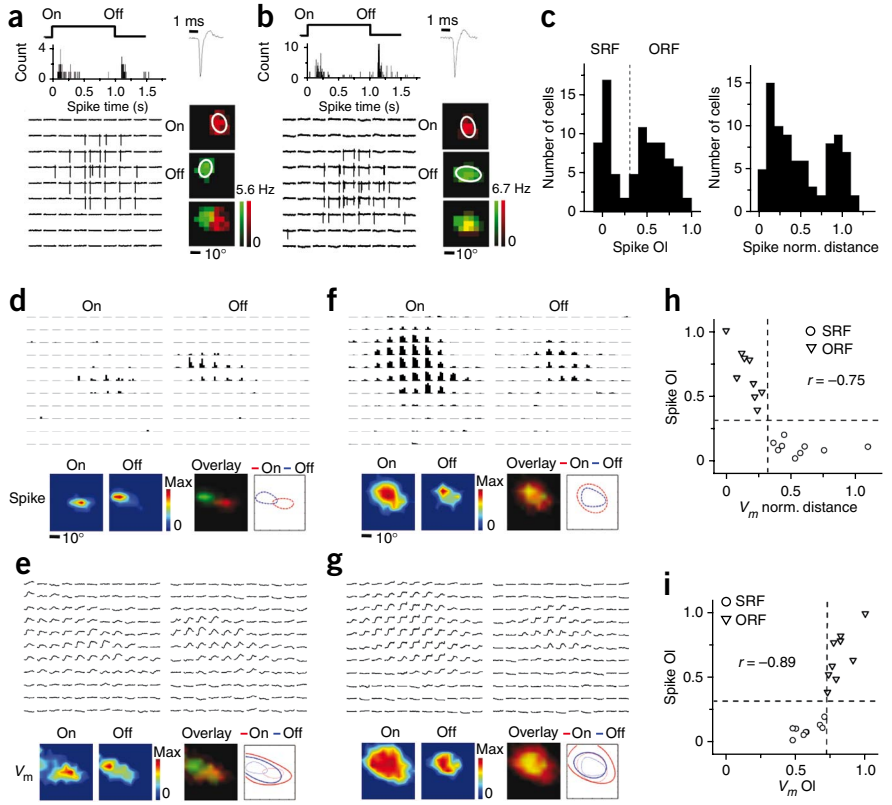

Figure 1 Membrane potential (V_m) responses underlying SRF and ORF structures in layer 2/3 of the mouse V1. (**a**,**b**) Example SRF (**a**) and ORF (**b**) cells. Top left, the peristimulus spike-time histograms for evoked spikes. On and Off mark the onset and offset of the stimuli respectively. Top right, the spike shape. Bottom left, each small trace (1.25 s) represents the recorded spike response (vertical deflections) in one trial to a unit stimulus shown at the corresponding spatial location. Bottom right, color maps of the spike subfields. The white ellipses depict the outlines of the spike subfields determined by Gaussian fittings. (**c**) Left, histogram of the overlap index of spike subfields (spike overlap index) for the recorded excitatory neurons. The dash line marks the overlap index of 0.33. Right, histogram of normalized distance between the peaks of spike On and Off subfields. (**d**) Spike receptive field for an example SRF cell. Top, each small trace (0.25 s) represents the peristimulus spike-time histogram for spike responses to a unit On or Off stimulus. Bottom, color maps and outlines of spike On/Off subfields. Color scale, 14.8 (On) and 39.1 Hz (Off). (**e**) V_m responses of the cell shown in **d**. Top, traces of average V_m responses. Bottom, color maps and outlines of V_m subfields. Color scale, 22 (On) and 26 mV (Off). (**f**,**g**) An example ORF cell. Data are presented as in **d** and **e**. Color scale, 42.3 and 21.5 Hz in **f** and 20 and 18 mV in **g**. (**h**) Spike overlap index versus normalized distance between the peaks of V_m subfields. The two dash lines (overlap index = 0.33, normalized distance = 0.32) separate SRF and ORF structures. r is the correlation coefficient. (**i**) Spike overlap index versus the overlap index of V_m subfields (V_m overlap index). The vertical and horizontal lines mark the V_m overlap index of 0.71 and the spike overlap index of 0.33 respectively.

subfields. Our results suggest an alternative synaptic mechanism for the generation of simple-cell receptive-field structure.

RESULTS

Subthreshold responses underlying spike receptive fields

Previous studies have suggested that simple- and complex-cell receptive fields primarily appear in layer 2/3 of the mouse V1 (refs. 28,29,31). We examined two examples of layer 2/3 excitatory neurons (**Fig. 1a**,**b**), which had spatially segregated and overlapped spike On and Off subfields, respectively, as detected by cell-attached recordings (see Online Methods). To quantify the spatial overlap between the On and Off subfields, we calculated an overlap index after fitting the subfields with two-dimensional Gaussian ellipses[6,8] (see Online Methods). The histogram of overlap index values revealed a dichotomy in the receptive field structures (Hartigan's dip test, $P < 0.05$, $n = 82$; **Fig. 1c**). An overlap index of 0.33 (the value for two identical subfields that are half separated and half overlapped) appeared to divide the cells into two groups. Cells with an overlap index less than 0.33 (~45%) were classified as neurons with segregated receptive-field structure (or SRF neurons). Otherwise, they were classified as neurons with overlapped receptive field structure (or ORF neurons)[31]. The normalized peak distance between the spike On and Off subfields[20] also had a bimodal distribution (Hartigan's dip test, $P < 0.05$, $n = 82$; **Fig. 1c**). In contrast with the SRF and ORF structures in layer 2/3 neurons, layer 4 neurons mostly responded only to one contrast (**Supplementary Fig. 1**), which is consistent with previous reports[28,29,31]. Because classic simple-cell receptive-field structures were primarily found in layer 2/3, we focused on layer 2/3 neurons.

To understand the patterns of subthreshold synaptic inputs underlying the SRF and ORF structures, we carried out current-clamp recordings to record both sub- and suprathreshold membrane potential responses. As shown for an example SRF cell, the subthreshold response regions were much larger than the spike subfields (**Fig. 1d**,**e**). Although the spike On and Off subfields were largely segregated, the subthreshold On and Off regions overlapped substantially (**Fig. 1e**). The peaks of the subthreshold subfields (where the maximum depolarizing response appears) were clearly offset spatially, with their locations being consistent with those of the spike subfields (**Fig. 1d**,**e**). In comparison, the subthreshold On and Off responses of an ORF cell exhibited a similarly large overlap (**Fig. 1f**,**g**), but without an apparent segregation between the peak depolarizing On and Off responses (**Fig. 1f**,**g**). In fact, the overlap index of spike subfields (spike overlap index) was strongly correlated with the normalized distance between the peaks of subthreshold subfields, decreasing monotonically with the increase of the latter (**Fig. 1h**). The SRF and ORF cells could be best separated by a normalized peak distance at 0.32, based on the Youden's index (see Online Methods). The spike overlap index was also strongly correlated with the overlap index of subthreshold subfields (see Online Methods; **Fig. 1i**), with a subthreshold overlap index of 0.71, at best, separating the SRF from ORF cells. These results suggest that the spatial pattern of subthreshold On and Off responses may predict the structure of the spike receptive field and that the spike threshold is required to generate the segregated spike On and Off subfields in the SRF cells. It should be noted that the level of the spike threshold was not associated with the receptive field type, as we found no significant

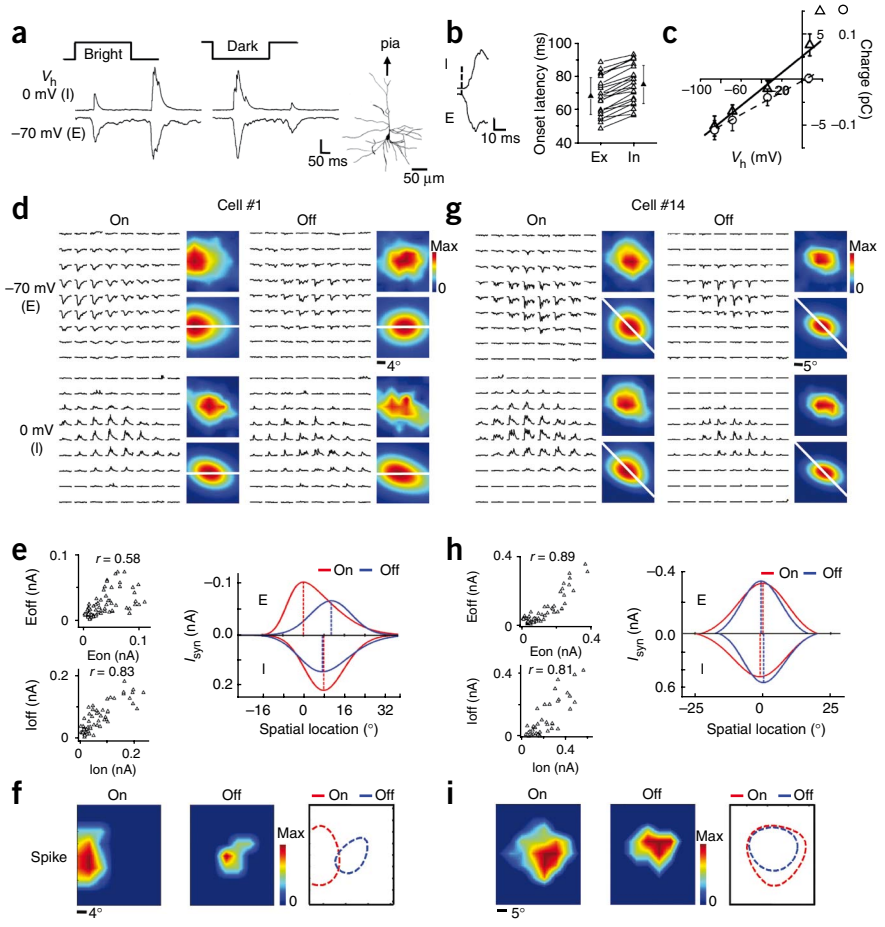

Figure 2 Synaptic subfields examined by voltage-clamp recordings. (**a**) Individual synaptic responses of a layer 2/3 pyramidal neuron to stimuli displayed at the same location. Scale bar indicates 118 (E) and 203 pA (I). Right, the reconstructed morphology of the cell. (**b**) Left, onset phase of synaptic responses. The onset of the excitatory response is marked by the dashed line. Scale bar indicates 80 (E) and 160 pA (I). Right, onset latencies of excitatory (Ex) and inhibitory (In) synaptic responses. Values from the same cell are connected with a line. The solid symbol indicates the mean and the error bars represent s.d. (**c**) *I-V* curves for a cell under white-noise stimulation. Synaptic charges were measured in a 0–5-ms (circle) and 10–150-ms (triangle) time window after the onset of excitatory synaptic responses. (**d**–**f**) A putative SRF cell. (**d**) Arrays of trial-averaged excitatory (E) and inhibitory (I) synaptic responses (0.35 s) to On and Off stimuli. Color maps are the smoothed (top) and skew-normal fitted (bottom) synaptic subfields. White lines pass through the peaks of the excitatory On and Off subfields. Color scale is 109, 73, 236 and 178 pA for Eon, Eoff, Ion and Ioff, respectively. (**e**) Left, correlation between the strengths of synaptic responses (Eon-Eoff, Ion-Ioff). Right, spatial tuning curves of the four synaptic inputs along the white lines in **d**. Dash lines mark their peaks. (**f**) Derived spike subfields of the same cell and their boundaries. Color scale is 25 (On) and 10 Hz (Off). (**g**–**i**) Synaptic subfields of a putative ORF cell. Data are presented as in **d**–**f**. Color scale is 381, 352, 560 and 412 pA for Eon, Eoff, Ion and Ioff, respectively, in **g**. Color scale is 25 (On) and 15 Hz (Off) in **i**.

difference between the SRF and ORF cells (*t* test, $P = 0.45$, 25.1 ± 2.6 mV for SRF cells and 23.9 ± 5.2 mV for ORF cells).

The observed membrane potential responses consisted mostly of depolarizing responses (**Fig. 1e**,**g**), which indicate the arrival of excitatory synaptic inputs. Thus, the largely overlapped depolarizing On and Off responses predict that the excitatory On and Off synaptic subfields may overlap substantially in both the SRF and ORF cells.

Subfields of excitatory and inhibitory inputs

To further elucidate the patterns of excitatory and inhibitory synaptic inputs, we carried out whole-cell voltage-clamp recordings to dissect synaptic excitation and inhibition (see Online Methods). We examined sample responses of a neuron to a bright or dark square flashed at the same location, recorded at two clamping voltages (**Fig. 2a**). The inward currents recorded at −70 mV and the outward currents at 0 mV were primarily contributed by excitatory and inhibitory synaptic inputs, respectively[25,26], with the inhibitory input temporally closely following the coactivated excitatory input[22–24,32] (**Fig. 2b**). The observed synaptic inputs were reasonably controlled by the somatic voltage clamp, as suggested by a linear *I-V* relationship and the derived reversal potential of the excitatory currents, which was close to 0 mV (**Fig. 2c** and **Supplementary Fig. 2**). This is probably a result of the proximity of the visually activated synapses to the soma of layer 2/3 neurons[33].

We mapped excitatory On and Off (Eon and Eoff) and inhibitory On and Off (Ion and Ioff) subfields by recording synaptic currents evoked by brief bright and dark stimuli while clamping the cell at −70 mV and 0 mV, respectively. For an example cell (cell #1; **Fig. 2d**), we examined the average traces of excitatory and inhibitory currents responding to all the On and Off stimuli and determined the distribution of the peak amplitude of the synaptic currents (**Fig. 2d**). We observed a considerable overlap between the Eon and Eoff, which was further demonstrated by the positive correlation between the strengths of the excitatory On and Off responses (**Fig. 2e**). Despite this overlap, it is clear that the peaks of the Eon and Eoff (where the strongest response is elicited) were spatially offset (**Fig. 2d**). Notably, the Ion and Ioff almost completely overlapped, as seen by a strong correlation between the inhibitory On and Off responses (**Fig. 2e**). To quantitatively describe the spatial relationship between each pair of the four synaptic subfields, we fitted the subfields with a two-dimensional skew-normal distribution function (see Online Methods; **Fig. 2d**), which better described the asymmetrical distribution of the synaptic strengths than the Gaussian function in some cells (**Supplementary Figs. 3** and **4**). We plotted the tuning curves for the four sets of synaptic inputs in the one-dimensional slice that passed through the peaks of both the Eon and Eoff (**Fig. 2e**). The peaks of the Eon and Eoff were segregated with a normalized distance of 0.53 (see Online Methods), whereas those of the Ion and Ioff were overlapped and located between the former two. The separation between the peaks of the Eon and Eoff was reminiscent of that of depolarizing subfields in the SRF cells (**Fig. 1e**). Indeed, the derived spike On and Off subfields (see Online Methods) of cell #1 had an almost complete segregation, suggesting that cell #1 is probably an SRF cell (**Fig. 2f**). In comparison, cell #14 had almost completely overlapped four synaptic

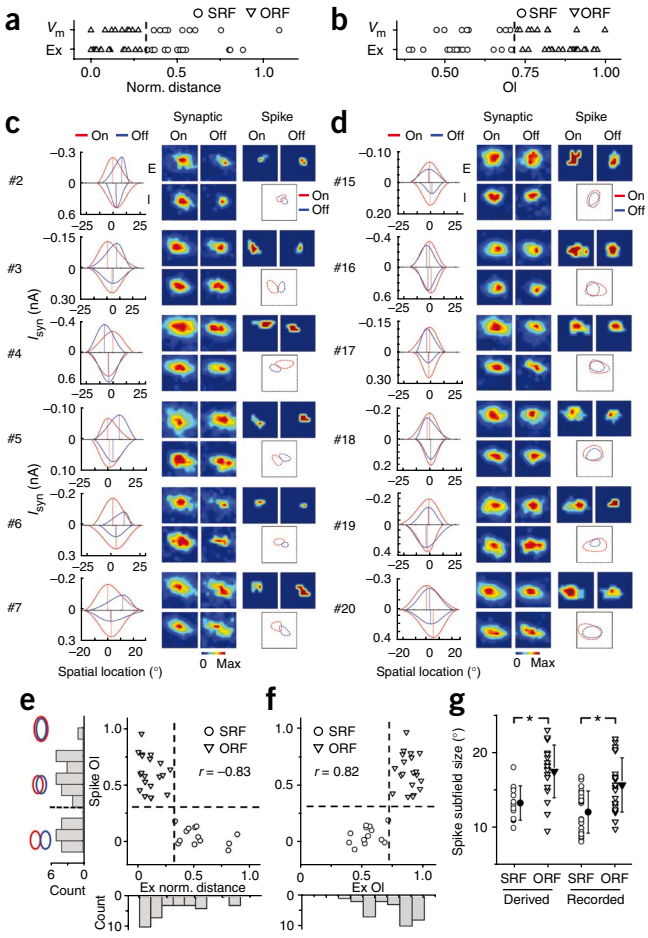

Figure 3 Grouping of cells on the basis of the structure of synaptic subfields. (**a**) The distributions of the normalized distances between the peaks of the V_m On/Off subfields and between the excitatory On/Off subfields (Ex). The two distributions were not different (Mann-Whitney test, $P = 0.14$). The dashed line marks normalized distance of 0.32, which we used to group the cells from voltage-clamp recordings. (**b**) The distributions of the overlap indexes of V_m and excitatory subfields (Mann-Whitney test, $P = 0.21$). The dashed line marks the overlap index of 0.71, which separated the cells from voltage-clamp recordings, as in **a**. (**c**) Synaptic subfields and derived spike subfields of six putative SRF cells. For each cell, the synaptic tuning curves in the slice that passes through the peaks of the Eon and Eoff are shown on the left, followed by the four synaptic subfields, the derived spike subfields and the superimposed outlines of fitted spike subfields (from left to right). Color scale: 337, 404, 543, 528 pA for synaptic subfields (Eon, Eoff, Ion, Ioff), 15, 10 Hz for spike On/Off subfields in cell #2; 163, 165, 288, 196 pA, 10, 15 Hz in cell #3; 280, 342, 638, 854 pA, 10, 10 Hz in cell #4; 122, 106, 142, 141 pA, 10, 10 Hz in cell #5; 225, 153, 245, 161 pA, 15, 20 Hz in cell #6; 311, 184, 412, 149 pA, 10, 5 Hz in cell #7. (**d**) Six putative ORF cells. Plots are organized in the same way as in **c**. Color scale: 74, 54, 141, 82 pA, 5, 10 Hz in cell #15; 398, 347, 595, 563 pA, 10, 10 Hz in cell #16; 141, 154, 298, 145 pA, 15, 15 Hz in cell #17; 187, 172, 218, 173 pA, 15, 15 Hz in cell #18; 232, 154, 356, 329 pA, 20, 5 Hz in cell #19; 280, 253, 415, 221 pA, 15, 15 Hz in cell #20. (**e**) Overlap index of derived spike subfields versus the normalized distance between the peaks of the Eon and Eoff for all recorded neurons ($n = 33$). The vertical and horizontal dashed lines mark the excitatory-subfield normalized distance of 0.32 and the spike overlap index of 0.33, respectively. Left, histogram of spike overlap index. The schematic drawings depict the extent of overlap between two identical subfields for overlap indexes of 0, 0.5 and 1. Bottom, histogram of the excitatory-subfield normalized distance. (**f**) Overlap index of derived spike subfields versus the overlap index between the Eon and Eoff. The vertical and horizontal dashed lines mark the excitatory-subfield overlap index of 0.71 and spike overlap index of 0.33, respectively. Bottom, the histogram of excitatory-subfield overlap index. (**g**) The distribution of the subfield size of the derived and recorded spike responses. The solid symbol indicates the mean and the error bars represent s.d. (* $P < 0.01$, t test).

subfields (**Fig. 2g**,**h**), with a good colocalization of all of their peaks (**Fig. 2h**). The derived spike On and Off subfields overlapped well, suggesting that cell #14 is probably an ORF cell (**Fig. 2i**).

Spatial relationships of synaptic subfields

Synaptic subfields were obtained for a total of 33 neurons. In all of these neurons, the four synaptic subfields substantially overlapped, but there was a relatively larger variation in the separation between the Eon and Eoff (**Supplementary Fig. 5**). According to spike response data (**Fig. 1c**), about half of these cells were potential SRF cells. To understand how different spatial patterns of synaptic inputs result in different spike receptive field structures, we roughly categorized the recorded cells into putative SRF and ORF cells. Because the spatial relationship between the Eon and Eoff primarily determined that of the subthreshold depolarizing responses (**Supplementary Fig. 6**) and the latter could predict the SRF/ORF structures (**Fig. 1h**,**i**), we applied the same separation criteria to the patterns of excitatory inputs to categorize cells (that is, SRF cells having normalized peak distance >0.32 or overlap index <0.71; **Fig. 3a**,**b**). Notably, the grouping was the same on the basis of either the overlap index or the normalized peak distance (**Fig. 3b**).

We examined more putative SRF and ORF cells (**Fig. 3c**,**d**). All of the putative SRF cells had similar patterns of synaptic inputs; there was a clear segregation between the peaks of the Eon and Eoff while the extent of these subfields substantially overlapped, and the peaks of the Ion and Ioff were largely colocalized and located somewhere between those of the Eon and Eoff. Their derived spike subfields showed a substantial segregation, supporting the categorization of them as SRF cells (**Fig. 3c**). In comparison, the putative ORF cells had more closely localized peaks of all the synaptic subfields and their derived spike subfields showed a large overlap (**Fig. 3d**). There was a strong correlation between the overlap index of derived spike subfields and the normalized peak distance or overlap index of the Eon and Eoff (**Fig. 3e**,**f**), consistent with our current-clamp recording results (**Fig. 1h**,**i**). The overlap index of derived spike subfields formed a bimodal distribution (Hartigan's dip test, $P < 0.05$; **Fig. 3e**), whereas the normalized peak distance or overlap index between the Eon and Eoff had a continuous distribution (Hartigan's dip test, $P = 0.38$ and $P = 0.25$; **Fig. 3e**,**f**), which is also consistent with the results of our cell-attached and current-clamp recordings (**Fig. 1c**,**h**,**i**). The distribution of the size of derived spike subfields was also similar to that of the extracellularly recorded receptive fields (**Fig. 3g**). These similarities suggest that the derived spike receptive fields had not underestimated or exaggerated the separation between the bona fide spike subfields.

The level of overlap between the Ion and Ioff, as well as between the excitatory and inhibitory subfields of the same contrast (Ex-In), was then compared between the putative SRF ($n = 13$) and ORF cells ($n = 20$) (**Fig. 4a**). Although the Eon and Eoff were more segregated in the SRF cells than in the ORF cells, the overlap between the Ion and Ioff was similarly large in the two groups. In the SRF cells, the average overlap index of Ex-In was higher than that of Eon-Eoff, but lower than that of Ion-Ioff, which is consistent with the notion that the peaks of the inhibitory subfields were usually located between those of the Eon and Eoff. To further illustrate the Ex-In relationship, we measured

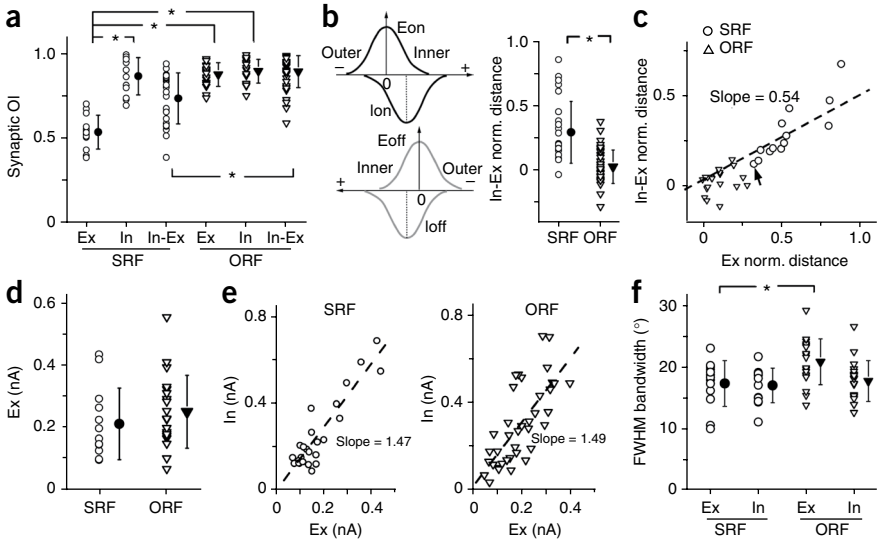

Figure 4 Summary of the spatial relationships between synaptic subfields. (**a**) The distributions of overlap indexes between the Eon and Eoff (Ex), the Ion and Ioff (In), and the excitatory and inhibitory subfields of the same contrast (In-Ex). The solid symbol indicates the mean and the error bars represent s.d. (* $P < 10^{-5}$, *t* test). (**b**) Left, we defined the inner side of an excitatory tuning curve as the one facing toward the other excitatory tuning curve of the opposite contrast. The value of the In-Ex distance is positive if the peak of the inhibitory field is located on the inner side of the excitatory field of the same contrast, but negative if it is on the outer side. Right, the distribution of the normalized In-Ex distance. The solid symbol indicates the mean and the error bars represent s.d. (* $P < 10^{-6}$, *t* test, $n = 26$ (SRF) and 40 (ORF)). (**c**) Normalized In-Ex distance (averaged for On and Off subfields) versus the normalized distance between the peaks of the Eon and Eoff. The dashed line is the best-fit linear regression line. The arrow indicates the only cell that would be grouped differently under TwoStep Cluster analysis. (**d**) The maximal amplitude of the excitatory currents. The solid symbol indicates the mean and the error bars represent s.d. ($P = 0.34$, *t* test). (**e**) The maximum strength of inhibitory input (In) versus that of excitatory input (Ex) in the same subfield. The dashed line shows the best-fit linear regression line. (**f**) The full-width at half-maximum bandwidth of excitatory and inhibitory spatial tuning curves. The solid symbol indicates the mean and the error bars represent s.d. (* $P = 0.02$, *t* test).

the normalized peak distance (**Fig. 4b**). In the SRF cells, almost all the values were positive, indicating that inhibition always peaked at the inner side of the excitatory subfield (**Fig. 4b**). On the other hand, in ORF cells, the relative locations of inhibitory peaks were random and were all close to 0, indicating that the inhibitory and excitatory peaks were essentially colocalized. The normalized peak distance for Ex-In was linearly correlated with that of Eon-Eoff, and was about half of the latter (**Fig. 4c**). On the basis of the distances of Ex-In and Eon-Eoff, the cells could be statistically separated into two clusters by TwoStep Cluster analysis, and the two clusters matched well with the cell-type categorization (concordance = 32/33). The two groups of cells did not differ significantly in their synaptic strengths (*t* test, $P = 0.34$) or in the size of their inhibitory subfields (*t* test, $P = 0.49$), although they differed slightly in the size of their excitatory subfields (**Fig. 4d–f**). This suggests that the spatial relationship between synaptic subfields primarily determines receptive field structures.

An inhibitory mechanism for the SRF structure

The largely overlapped excitatory and inhibitory subfields that we observed indicated that the inhibition would spatiotemporally interact with the excitation. To determine the effect of inhibition on spike receptive field structures, we derived spike receptive fields in the absence of inhibitory inputs (see Online Methods). For the SRF cells, the spike On and Off subfields derived from excitatory inputs alone showed substantial overlaps, whereas the integration of inhibition resulted in largely increased On/Off segregation (**Fig. 5a** and **Supplementary Fig. 7**). In the ORF cells, the spike subfields were only reduced in size, with no apparent improvement in the segregation. Thus, the small segregation between the Eon and Eoff cannot fully account for a complete segregation of spike subfields. Instead, inhibition is crucial for determining their spatial distinctiveness.

How does inhibition shape spike receptive field structures? On the basis of the largely overlapping, but subtly mismatched, spatial relationship between the excitatory and inhibitory inputs to SRF cells (**Fig. 5b**), we propose that inhibition can enhance the distinctiveness of spike On and Off subfields through an asymmetric suppression effect. Because of the large overlap between Eon and Eoff, the spike threshold alone may not be sufficient to generate a complete On/Off segregation (**Fig. 5b**). The integration of inhibition will reduce the size of spike subfields by suppressing the level of the membrane excitation (**Fig. 5b**). More importantly, as a result of the locations of the inhibitory peaks at the inner sides of the excitatory tunings, the inhibition will exert a stronger suppression effect on the inner side of the membrane potential tuning curve than on its outer side. This can result in a more effective separation of suprathreshold On and Off response regions (**Fig. 5b**). For example cell #1, a putative SRF cell (**Fig. 2e**), the inclusion of inhibition markedly changed the shape of the On membrane potential tuning curve, with a strong suppression on its inner side (**Fig. 5c**). This reshaping greatly increased the distinctiveness of the On and Off tunings, resulting in almost completely segregated spike subfields (**Fig. 2f**). On the contrary, for the putative ORF cell (the cell #14; **Fig. 2h**), inhibition had little effect on the distinctiveness of the On and Off tunings (**Fig. 5d**). As a result, the spike On and Off subfields remained overlapping after the integration of inhibition (**Fig. 2i**).

We examined the asymmetric shaping effect on the On/Off tunings (**Fig. 5e**). In the SRF cells, the half-peak width of the membrane potential tuning was significantly reduced (paired *t* test, $P < 0.01$) after the integration of inhibition at the inner side, but not at the outer side. As a result, the spike subfield boundary shrank to a larger degree at the inner side than the outer side (**Fig. 5f**). In contrast, the shape of membrane potential tunings was largely unchanged in the presence of inhibition in the ORF cells (**Fig. 5e**). Thus, empowered by the slightly mismatched spatial relationship between excitation and inhibition, the inhibition can exert a powerful asymmetric shaping effect on the On/Off tunings in SRF cells, leading to a more pronounced reduction in the overlap index of spike subfields (**Fig. 5g**). This effect greatly increases the functional difference between the two groups of cells.

Modeling the generation of the SRF structure

Our results identify two essential factors for the generation of On/Off segregation: the slightly segregated Eon and Eoff and a specific mismatch between the excitation and inhibition. To further understand how spatial patterns of synaptic inputs may contribute to spike receptive

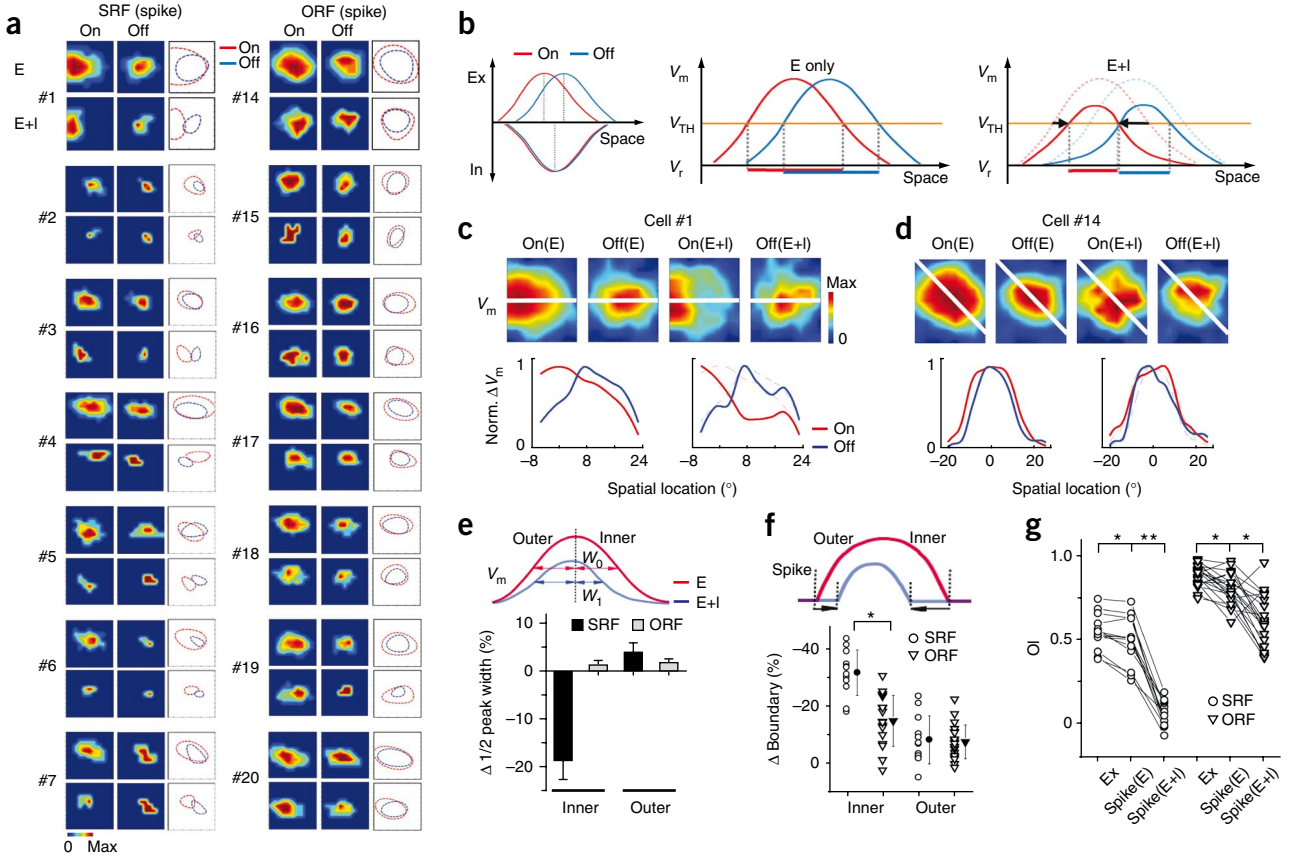

Figure 5 The inhibitory mechanism for the generation of the SRF structure. (**a**) Derived spike subfields without (E) and with the integration of inhibition (E+I) of the cells in **Figures 2** and **3**. Dashed curves represent the outlines of the subfields. Color scale (On(E), Off(E), On(E+I) and Off(E+I)): cell #1, 30, 25, 25, 10 Hz; cell #2, 20, 15, 15, 10 Hz; cell #3, 25, 20, 10, 15 Hz; cell #4, 25, 20, 10, 10 Hz; cell #5, 15, 10, 10, 10 Hz; cell #6, 25, 20, 15, 20 Hz; cell #7, 15, 10, 10, 5 Hz; cell #14, 35, 20, 25, 15 Hz; cell #15, 20, 15, 5, 10 Hz; cell #16, 30, 15, 10, 10 Hz; cell #17, 25, 20, 15, 15 Hz; cell #18, 20, 15, 15, 15 Hz; cell #19, 30, 20, 20, 5 Hz; cell #20, 20, 15, 15, 15 Hz. (**b**) Inhibition is involved in the generation of SRFs. Left, the spatial tuning curves of excitatory and inhibitory inputs. The peak locations are marked by dotted lines. Middle, the spatial tuning curves of V_m responses without inhibition. V_{TH}, spike threshold; V_r, resting potential. The thick red and blue lines below the tuning curves represent the one-dimensional regions of the suprathreshold On/Off responses, respectively. Note that they overlap substantially. Right, the V_m tuning curves after integrating inhibition (solid curves) overlaid with the tuning curves without inhibition (dashed). The suprathreshold On/Off response regions are now segregated. Arrows indicate the shrinkage of suprathreshold subfield boundaries. (**c**) Top, color maps of V_m responses derived without (E) and with (E+I) integrating inhibition for cell #1. Color scales represent 47, 40, 39 and 26 mV, from left to right. The white line is defined as in **Figure 2d**. Bottom, normalized spatial tuning curves of V_m responses along the white line in the absence (left) and presence (right, solid) of inhibition. There was a strong suppression of the right part of the On tuning curve. (**d**) Similar plots for cell #14. Color scales represent 54, 53, 32 and 36 mV, from left to right. (**e**) The percentage change in the half-peak width of the V_m tuning curve after integrating inhibition. Top, schematic drawing of V_m tuning curves before and after integrating inhibition, with the half-peak widths at the inner side labeled by W_0 and W_1, respectively. The percentage change is then defined as $(W_1 - W_0)/W$, where W is the full-width at half-maximum of the tuning curve without inhibition. Error bars represent s.e.m. (**f**) The percentage shift of spike subfield boundaries after integrating inhibition. Arrows in the schematic drawings depict the boundary shift on the inner and outer side. The absolute value was divided by the size of spike subfields without inhibition to obtain the percentage shift. (**g**) Overlap indexes between Eon and Eoff (Ex) and between spike On/Off subfields derived without (spike(E)) and with inhibition (spike(E+I)). Values for the same cell are connected with lines. * $P < 0.005$, ** $P < 0.0001$, paired t test.

field structures, we applied a simple neuron model on the basis of the parameters derived from our experimental data (**Fig. 6a**; see Online Methods). Consistent with our experimental data, the slightly segregated excitatory On and Off inputs were not sufficient to generate the SRF structure, whereas integrating inhibition resulted in an almost complete On/Off segregation (**Fig. 6a**). The level of inhibition strongly affected the level of the On/Off segregation. With the synaptic distributions and the strength of excitation fixed, an increase in the strength of inhibition led to a monotonic enhancement of the On/Off segregation, as indicated by the decrease in the overlap index of spike subfields (**Fig. 6b**).

Next, we systematically varied the spatial relationships between synaptic subfields. By fixing the inhibitory subfields and gradually increasing the separation between the Eon and Eoff, we found that inhibition most effectively reduced the spike overlap index when the separation between the Eon and Eoff was small (6° apart or overlap index of 0.72; **Fig. 6c**). On the other hand, with the positions of the Eon and Eoff fixed, the inhibitory subfields had the largest effect of reducing spike overlap index when they were located right in the middle of the Eon and Eoff (**Fig. 6d**). We further examined the asymmetric inhibitory shaping by sliding an inhibitory subfield away from its excitatory field of the same contrast toward that of the opposite contrast (**Fig. 6e**). By integrating inhibition, the shrinkage of the spike subfield boundary at the inner side was larger than the outer side and reached the maximum when the inhibitory subfield shifted by ~5° (**Fig. 6e**). These simulation results further indicate that a small spatial

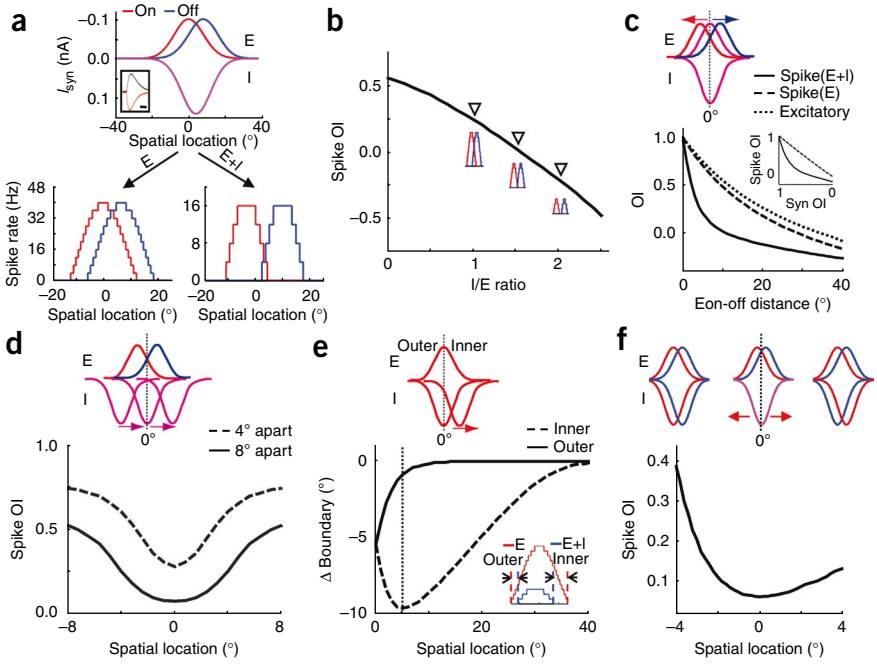

Figure 6 Modeling of the manner in which spatial relationships between synaptic subfields affect the segregation of spike On/Off subfields. (**a**) Top, the spatial tuning curves of synaptic currents (I_{syn}) used in the model. Inset, the temporal profiles of evoked excitatory (red) and inhibitory currents (black). Scale bar represents 125 ms. Bottom, the tuning curves of spike responses without (left) and with inhibition (right). (**b**) With the strength of excitation fixed at 0.1 nA, the spike overlap index (spike OI) decreased as the ratio between the strengths of inhibition and excitation (I/E ratio) increased. Inset, spike tuning curves at I/E ratios of 1, 1.5 and 2. (**c**) Top, modeling scenario. The excitatory On (red) and Off (blue) subfields were initially colocalized with the overlapping inhibitory fields (purple) and then moved away from each other at the same speed. Bottom, overlap indexes between the Eon and Eoff (dotted) and between spike subfields without (dashed) and with inhibition (solid) versus the distance between the peaks of the Eon and Eoff. Inset, spike overlap index versus the overlap index between the Eon and Eoff (Syn OI). (**d**) Top, the peaks of the Eon and Eoff were separated by 4° (dashed) or 8° (solid) and the overlapping inhibitory subfields moved together across different locations. Bottom, spike overlap index versus the spatial location of the inhibitory fields. (**e**) Top, the Ion was initially colocalized with the Eon and then moved in the direction of the Eoff (data not shown). Bottom, shift of the spike subfield boundary after integrating inhibition versus the location of the Ion peak. The dotted line marks the location of inhibitory subfield (~5°) where it shrinks the inner boundary most. Inset, spike tuning curves without (red) and with inhibition (blue) when the Ion peak is located at 4°. Arrows mark the boundary shifts on the two sides. (**f**) Top, the positions of the excitatory subfields were fixed, with an 8° separation. The initially overlapping inhibitory subfields moved in opposite directions to form either exquisitely balanced excitation and inhibition (left) or an antagonistic configuration similar to the push-pull configuration (right). Bottom, spike overlap index versus the location of the Ion peak, which was equal to –4°, 0° and 4° for the three scenarios described above, respectively.

shift of the inhibitory tuning results in a greatly enhanced separation between the spike On and Off responses through the asymmetric shaping effect.

DISCUSSION

The spatial patterns of excitatory and inhibitory On and Off inputs that we found are apparently different from those of the push-pull model. In the push-pull circuit, cortical inhibition is spatially antagonistic to excitation and the On/Off segregation is mainly determined by the spatial segregation of excitatory On and Off inputs. We found that neurons with either segregated or overlapped spike On and Off subfields all had substantial overlaps between all four of the synaptic subfields. The segregated receptive field structure of SRF cells was created by a specific spatial arrangement of synaptic subfields: the slight separation between the peaks of excitatory On and Off subfields and the intervening inhibitory subfields. The slightly separated excitatory On and Off subfields were not sufficient to generate the SRF structure. Instead, the small mismatch between the excitation and inhibition led to an asymmetric inhibitory shaping of the On and Off tunings, resulting in a strong suppression in their common region and a greatly increased segregation of spike subfields. As suggested by the results of our modeling study, the level of the On/Off segregation was sensitive to the relative location of inhibitory subfields (**Fig. 6f**). In fact, in a push-pull–like configuration (with more separation between the excitation and inhibition of the same contrast), inhibition does not further improve the segregation (**Fig. 6f**). The substantial spatial overlap between excitation and inhibition in visual cortical neurons is reminiscent of the balanced excitation and inhibition that has been observed in the auditory and somatosensory cortices[22–24,26].

The different synaptic organizations between the push-pull model and the model in this study could be a result of the species difference, as SRF cells are primarily found in layer 2/3 in the mouse V1 (refs. 27–31), whereas simple cells appear in the thalamo-recipient layers 4 and 6 in cats[1,6,21]. Nonetheless, the patterns of synaptic inputs that we observed provide a potential explanation for the previous observations in cats that blocking intracortical inhibition leads to a loss of On/Off segregation[11,12] and that inhibitory conductances can be activated by both On and Off stimuli in both On and Off subfields[10]. In addition, our data suggest that On/Off receptive field structures are sensitive to the delicate relationship between the spatial tunings of the four synaptic inputs and may potentially be modified by neuronal activity[34] or changed developmentally, as excitatory and inhibitory tuning patterns can be developmentally regulated[35,36]. The overlap-but-mismatched pattern of synaptic subfields is able to produce seemingly antagonistic On and Off responses (**Supplementary Fig. 8**). This is because the spatial mismatch between the excitatory and inhibitory tunings can result in relatively stronger inhibition at one side of the excitatory tuning. Thus, the push-pull–like phenomenon could be generated from synaptic circuits other than the push-pull circuit. The inhibitory inputs to most of layer 2/3 neurons in the mouse V1 are mainly from local inhibitory neurons[37,38]. The overlapped Ion and Ioff suggest that inhibitory neurons with SRF structures may not be required to provide input to excitatory SRF cells. Indeed, we recently found that layer 2/3 inhibitory neurons in the mouse V1 mostly have overlapping spike On and Off subfields[31].

The separation between excitatory On and Off subfields formed a continuous distribution among our recorded cells, consistent with a previous observation of membrane potential responses in cats[16]. It was recently proposed that the nonlinearity of spike mechanism can

create a dichotomy between simple and complex cells from a continuous distribution of intracellular properties[14–16]. Our results suggest that, although the intrinsic neuronal mechanism of spike thresholding reduces the overlap between On and Off responses, the dichotomy of receptive field structures becomes much more evident after the incorporation of inhibition (**Figs. 3e**, **5g** and **Supplementary Fig. 7**). Thus, besides the spike threshold, the inhibitory shaping may be an indispensable mechanism contributing to the dichotomy of the spatial organizations of receptive fields. Taken together, our results suggest an alternative synaptic circuitry mechanism by which a fine-tuning of spatial patterns of synaptic inputs can create the simple-cell receptive field, as well as the dichotomy in receptive field structures.

METHODS

Methods and any associated references are available in the online version of the paper at http://www.nature.com/natureneuroscience/.

Note: Supplementary information is available on the Nature Neuroscience website.

ACKNOWLEDGMENTS

We thank A. Sampath and D. Li for their helpful suggestions. This work was supported by grants to H.W.T. from the US National Institutes of Health (EY018718 and EY019049) and The Karl Kirchgessner Foundation. L.I.Z. is supported by the Searle Scholar Program, the Klingenstein Foundation, and the David and Lucile Packard Foundation.

AUTHOR CONTRIBUTIONS

B.-h.L. and P.L. performed most of the experiments and B.-h.L. carried out the data analysis. B.-h.L. and Y.J.S. carried out the modeling. Y.-t.L. helped with current-clamp recording experiments. H.W.T. and L.I.Z. designed the experiments and wrote the manuscript.

Published online at http://www.nature.com/natureneuroscience/.
Reprints and permissions information is available online at http://www.nature.com/reprintsandpermissions/.

1. Hubel, D.H. & Wiesel, T.N. Receptive fields, binocular interaction and functional architecture in the cat's visual cortex. *J. Physiol. (Lond.)* **160**, 106–154 (1962).
2. Heggelund, P. Quantitative studies of the discharge fields of single cells in cat striate cortex. *J. Physiol. (Lond.)* **373**, 277–292 (1986).
3. Hirsch, J.A., Alonso, J.M., Reid, R.C. & Martinez, L.M. Synaptic integration in striate cortical simple cells. *J. Neurosci.* **18**, 9517–9528 (1998).
4. Troyer, T.W., Krukowski, A.E., Priebe, N.J. & Miller, K.D. Contrast-invariant orientation tuning in cat visual cortex: feedforward tuning and correlation-based intracortical connectivity. *J. Neurosci.* **18**, 5908–5927 (1998).
5. Miller, K.D. Understanding layer 4 of the cortical circuit: a model based on cat V1. *Cereb. Cortex* **13**, 73–82 (2003).
6. Hirsch, J.A. & Martinez, L.M. Circuits that build visual cortical receptive fields. *Trends Neurosci.* **29**, 30–39 (2006).
7. Ferster, D. & Miller, K.D. Neural mechanisms of orientation selectivity in the visual cortex. *Annu. Rev. Neurosci.* **23**, 441–471 (2000).
8. Hirsch, J.A. *et al.* Functionally distinct inhibitory neurons at the first stage of visual cortical processing. *Nat. Neurosci.* **6**, 1300–1308 (2003).
9. Ferster, D. Spatially opponent excitation and inhibition in simple cells of the cat visual cortex. *J. Neurosci.* **8**, 1172–1180 (1988).
10. Borg-Graham, L.J., Monier, C. & Frégnac, Y. Visual input evokes transient and strong shunting inhibition in visual cortical neurons. *Nature* **393**, 369–373 (1998).
11. Sillito, A.M. The contribution of inhibitory mechanisms to the receptive field properties of neurones in the striate cortex of the cat. *J. Physiol. (Lond.)* **250**, 305–329 (1975).
12. Nelson, S., Toth, L., Sheth, B. & Sur, M. Orientation selectivity of cortical neurons during intracellular blockade of inhibition. *Science* **265**, 774–777 (1994).
13. Carandini, M. & Ferster, D. Membrane potential and firing rate in cat primary visual cortex. *J. Neurosci.* **20**, 470–484 (2000).
14. Mechler, F. & Ringach, D.L. On the classification of simple and complex cells. *Vision Res.* **42**, 1017–1033 (2002).
15. Abbott, L.F. & Chance, F.S. Rethinking the taxonomy of visual neurons. *Nat. Neurosci.* **5**, 391–392 (2002).
16. Priebe, N.J., Mechler, F., Carandini, M. & Ferster, D. The contribution of spike threshold to the dichotomy of cortical simple and complex cells. *Nat. Neurosci.* **7**, 1113–1122 (2004).
17. Palmer, L.A. & Davis, T.L. Receptive-field structure in cat striate cortex. *J. Neurophysiol.* **46**, 260–276 (1981).
18. Dean, A.F. & Tolhurst, D.J. On the distinctness of simple and complex cells in the visual cortex of the cat. *J. Physiol. (Lond.)* **344**, 305–325 (1983).
19. Jones, J.P. & Palmer, L.A. The two-dimensional spatial structure of simple receptive fields in cat striate cortex. *J. Neurophysiol.* **58**, 1187–1211 (1987).
20. Mata, M.L. & Ringach, D.L. Spatial overlap of ON and OFF subregions and its relation to response modulation ratio in macaque primary visual cortex. *J. Neurophysiol.* **93**, 919–928 (2005).
21. Martinez, L.M. *et al.* Receptive field structure varies with layer in the primary visual cortex. *Nat. Neurosci.* **8**, 372–379 (2005).
22. Zhang, L.I., Tan, A.Y.Y., Schreiner, C.E. & Merzenich, M.M. Topography and synaptic shaping of direction selectivity in auditory cortex. *Nature* **424**, 201–205 (2003).
23. Wehr, M. & Zador, A.M. Balanced inhibition underlies tuning and sharpens spike timing in auditory cortex. *Nature* **426**, 442–446 (2003).
24. Higley, M.J. & Contreras, D. Balanced excitation and inhibition determine spike timing during frequency adaptation. *J. Neurosci.* **26**, 448–457 (2006).
25. Liu, B.H., Wu, G.K., Arbuckle, R., Tao, H.W. & Zhang, L.I. Defining cortical frequency tuning with recurrent excitatory circuitry. *Nat. Neurosci.* **10**, 1594–1600 (2007).
26. Wu, G.K., Arbuckle, R., Liu, B.H., Tao, H.W. & Zhang, L.I. Lateral sharpening of cortical frequency tuning by approximately balanced inhibition. *Neuron* **58**, 132–143 (2008).
27. Dräger, U.C. Receptive fields of single cells and topography in mouse visual cortex. *J. Comp. Neurol.* **160**, 269–290 (1975).
28. Mangini, N.J. & Pearlman, A.L. Laminar distribution of receptive field properties in the primary visual cortex of the mouse. *J. Comp. Neurol.* **193**, 203–222 (1980).
29. Métin, C., Godement, P. & Imbert, M. The primary visual cortex in the mouse: receptive field properties and functional organization. *Exp. Brain Res.* **69**, 594–612 (1988).
30. Niell, C.M. & Stryker, M.P. Highly selective receptive fields in mouse visual cortex. *J. Neurosci.* **28**, 7520–7536 (2008).
31. Liu, B.H. *et al.* Visual receptive field structure of cortical inhibitory neurons revealed by two-photon imaging guided recording. *J. Neurosci.* **29**, 10520–10532 (2009).
32. Tan, A.Y.Y., Zhang, L.I., Merzenich, M.M. & Schreiner, C.E. Tone-evoked excitatory and inhibitory synaptic conductances of primary auditory cortex neurons. *J. Neurophysiol.* **92**, 630–643 (2004).
33. Petreanu, L., Mao, T., Sternson, S.M. & Svoboda, K. The subcellular organization of neocortical excitatory connections. *Nature* **457**, 1142–1145 (2009).
34. Debanne, D., Shulz, D.E. & Fregnac, Y. Activity-dependent regulation of 'on' and 'off' responses in cat visual cortical receptive fields. *J. Physiol. (Lond.)* **508**, 523–548 (1998).
35. Tao, H.W. & Poo, M.M. Activity-dependent matching of excitatory and inhibitory inputs during refinement of visual receptive fields. *Neuron* **45**, 829–836 (2005).
36. Liu, Y., Zhang, L.I. & Tao, H.W. Heterosynaptic scaling of developing GABAergic synapses: dependence on glutamatergic input and developmental stage. *J. Neurosci.* **27**, 5301–5312 (2007).
37. Dantzker, J.L. & Callaway, E.M. Laminar sources of synaptic input to cortical inhibitory interneurons and pyramidal neurons. *Nat. Neurosci.* **3**, 701–707 (2000).
38. Yoshimura, Y. & Callaway, E.M. Fine-scale specificity of cortical networks depends on inhibitory cell type and connectivity. *Nat. Neurosci.* **8**, 1552–1559 (2005).

ONLINE METHODS

Animal preparation. All experimental procedures used in this study were approved by the Animal Care and Use Committee of the University of Southern California. Female adult mice (12–16 weeks, C57BL/6) were anesthetized with urethane (1.2 g per kg of body weight) and sedative chlorprothixene (0.05 ml of 4 mg ml^{-1}), as previously described[28–31,39]. Lactated Ringer's solution was administrated at 3 ml per kg per h to prevent dehydration. The mouse's body temperature was maintained at ~37.5° by a heating pad (Havard Apparatus). A trachotomy was performed to maintain a clear airway and a ventilator (Havard Apparatus) was connected. Cerebrospinal fluid draining was performed to prevent the cortex from swelling. The mouse was placed in a custom-built stereotaxic holder. The part of the skull and dura mater (~1 × 1 mm) over the V1 was removed. Artificial cerebrospinal fluid solution (140 mM NaCl, 2.5 mM KCl, 2.5 mM $CaCl_2$, 1.3 mM $MgSO_4$, 1.0 mM NaH_2PO4, 20 mM HEPES and 11 mM glucose, pH 7.4) was applied onto the exposed cortical surface when necessary. Throughout the surgical procedure, the lids were sutured. After surgery, the right eyelid was reopened and drops of 30k silicone oil were applied to prevent the eye from drying. The whole procedure of receptive field mapping was finished in 25 min. Previous studies found that the drift of the measured receptive field in nonparalyzed mice was negligible within 1 h compared with the average receptive field size[27–29,39]. Our cell-attached recording also showed that the drift of the measured receptive field of single unit was never more than 2–3° per h, indicating that the largely overlapped excitation was not a result of the eye movement.

***In vivo* cell-attached, whole-cell current-clamp and whole-cell voltage-clamp recording.** Whole-cell recording (Axopatch 200B) was performed as described previously[25,26,40,41]. The patch pipette had a tip opening of ~2 μm (4.5–6 MΩ). The intrapipette solution for voltage-clamp recording contained 125 mM cesium gluconate, 5 mM TEA-Cl, 4 mM MgATP, 0.3 mM GTP, 8 mM phosphocreatine, 10 mM HEPES, 10 mM EGTA, 2 mM CsCl, 1.5 mM QX-314, 0.5% biocytin and 0.75 mM MK-801 (pH 7.25). For the current-clamp recording, the solution contained 130 mM potassium gluconate, 2 mM KCl, 1 mM $CaCl_2$, 4 mM MgATP, 0.3 mM GTP, 8 mM phosphocreatine, 10 mM HEPES, 11 mM EGTA and 0.5% biocytin (pH 7.25). To prevent pulsation, we applied 3.25% agarose to the exposed cortex before recording. The whole-cell and pipette capacitance were completely compensated for and the initial series resistance (20–50 MΩ) was compensated for by 50–60% to achieve an effective series resistance of 10–25 MΩ. Signals were filtered at 2 kHz for voltage clamp and 5 kHz for current clamp and sampled at 10 kHz. No current injection was applied under the current-clamp mode. Only neurons with resting membrane potentials lower than −55 mV and stable series resistance (less than 15% change from the beginning of the recording) were used for further analysis. Histological staining of some of the recorded cells indicated that our whole-cell recording method biased sampling toward pyramidal neurons, consistent with previous results[25,26,40,41]. The recorded cell was first clamped at −70 mV, which is around the reversal potential of inhibitory currents, to obtain evoked excitatory currents. The cell was then clamped at 0 mV, which is around the reversal potential of excitatory currents, to obtain evoked inhibitory currents. Loose-patch cell-attached recording was performed as described previously[26,31,32]. Glass electrodes with the same opening size containing artificial cerebrospinal fluid were used. Instead of a giga-seal, a 100–250-MΩ seal was formed on the targeted neuron. All of the neurons recorded under this condition showed regular-spike property, consistent with sampling bias toward excitatory neurons. The pipette capacitance was completely compensated for, minimizing the distortion of the recorded spike shape. The spike signal was filtered at 10 kHz and sampled at 20 kHz. The apparent lack of hyperpolarizing responses in current-clamp recordings may be attributed to the fact that the reversal potential of inhibitory currents was close to the resting membrane potentials of the recorded cells.

Visual stimulation. Software for data acquisition and visual stimulation were custom-developed with LabView (National Instrument) and MATLAB (Mathworks), respectively. Visual stimuli were provided by a 34.5- × 25.9-cm monitor (refresh rate of 120 Hz, mean luminance of ~10 cd m^{-2}) placed 0.25 m away from the right eye. The mouse eye has a much larger depth of focus (±10 diopters) than that of cats (±0.3 diopters), which means that the change in image quality of an object located from infinity to a distance of 0.1 m cannot be discerned by the mouse eye[42–44]. Thus, 0.25 m from the mouse eye is equivalent to infinity. The center of monitor was placed at 45° azimuth and 0° elevation[39], and it covered ±35° horizontally and ±27° vertically of the mouse visual field. To map spatial receptive field, we used two types of stimulation. For the first type, a set of bright squares (contrast 90%) in an 11 × 11 grid (grid size of 4–5°) were displayed individually in a pseudo-random sequence, with a 1-s duration and a 1-s interstimulus interval. The On and Off subfields were derived from the responses to the onset and offset of the bright squares, respectively[17]. For the second type, a set of bright and dark squares over a gray background (contrast of 70% and −70%, respectively) in an 11 × 11 grid (grid size of 4–5°) were flashed individually (duration of 200 ms, interstimulus interval of 300 ms) in a pseudo-random sequence, similar to the sparse stimuli used in the cat visual cortex[3,8,16,19]. Each location was stimulated 3–6 times for synaptic receptive field and ≥5 times for spike receptive fields, and the same number of On and Off stimuli were applied. The On and Off subfields were derived from responses to the onset of bright and dark squares, respectively. To be consistent with previous studies, we mapped synaptic subfields with the second type of stimulation. Spike receptive fields mapped with the two types of stimulation were similar and were pooled. The size of the stimulus was relatively small compared with that of the synaptic subfield, which was usually more than 35° (**Fig. 3c**,**d**). The mean overlap between synaptic subfields in the SRF cells was larger than 25° (**Supplementary Fig. 9**). This large overlap between synaptic subfields cannot be explained by the possibility that some stimuli occur on the boundary between synaptic subfields.

Data analysis. Spikes were sorted offline after cell-attached recording. For the first type of stimulation, On and Off spike responses were measured in a 70–250-ms and a 1,070–1,250-ms window after the onset of stimuli, respectively. For the second type of stimulation, spikes were counted in a 70–220-ms window after the onset of stimuli. The baseline activity was subtracted from stimulus-evoked spike rates. Responses in which the peak firing rate was threefold larger than the s.d. of baseline activity were considered to be significant. The averaged firing rate was used to make receptive field color maps, which were normally smoothed with bilinear interpolation.

For intracellular recording, the peak amplitudes of synaptic responses (average from three to six trials) or V_m responses (averaged from more than eight trials after removing spikes with an 8-ms median filter[45]) were used for the receptive field color maps (smoothed with bilinear interpolation) and the spatial correlation plots. Excitatory and inhibitory synaptic conductances were derived as described previously[10,22,23,25,26,32]:

$$I(t) = G_r\left(V_m(t) - E_r\right) + G_e(t)\left(V_m(t) - E_e\right) + G_i(t)\left(V_m(t) - E_i\right)$$

where I is the amplitude of current at any time point, G_r and E_r are the resting leak conductance and resting membrane potential, respectively, and were derived from the baseline current of each recording, G_e and G_i are the excitatory and inhibitory synaptic conductance, respectively, V_m is the membrane potential, and E_e (0 mV) and E_i (–70 mV) are the reversal potentials. $V_m(t)$ is corrected by $V_m(t) = V_h - R_s I(t)$, where R_s was the effective series resistance and V_h is the applied holding voltage. A 12-mV junction potential was corrected. By holding the recorded cell at two different voltages, G_e and G_i were calculated from the equation. G_e and G_i reflect the strength of pure excitatory and inhibitory synaptic inputs, respectively. The visually evoked synaptic currents are primarily mediated by AMPA and $GABA_A$ receptors.

In the voltage-clamp recordings, we were not able to experimentally examine the spike responses of the recorded cell because our intracellular solution contained QX-314, a blocker of voltage-dependent Na^+ channels, to increase the clamping quality. Nevertheless, we could estimate membrane potential and spike responses by feeding the experimentally derived excitatory and inhibitory conductances into an integrate-and-fire model[23,25,46],

$$V_m(t+dt) = -\frac{dt}{C}\left[G_e(t)\left(V_m(t) - E_e\right) + G_i(t)\left(V_m(t) - E_i\right) + G_r\left(V_m(t) - E_r\right)\right] + V_m(t)$$

where $V_m(t)$ is the membrane potential at time t, C is the whole-cell capacitance, G_r is the resting leak conductance and E_r is the resting membrane potential (−65 to −60 mV). To simulate spike response, the spike threshold was set 20 mV above the resting membrane potential and we used a 10-ms refractory period. C was measured during experiments and G_r was calculated from the

equation $G_r = \frac{CG_m}{C_m}$, where G_m, the specific membrane conductance, is 2×10^{-5} S cm^{-2}, and C_m, the specific membrane capacitance, is 10^{-6} F cm^{-2} (ref. 47). The derived spike receptive fields were similar to those recorded directly (**Fig. 3e,g**), suggesting that the integrate-and-fire model provides reasonable estimations of spike receptive fields.

To quantify the separation between On and Off subfields, we calculated an overlap index[6,8,21,48] for cells exhibiting both On and Off responses. The overlap index is defined as:

$$OI = \frac{W_1 + W_2 - d}{W_1 + W_2 + d}$$

where d is the distance between the peaks of two subfields, OI is the overlap index, and W_1 and W_2 are the half widths on the inner side of the two subfields, respectively, defined as the segment of the line connecting the two subfield peaks between the peak and boundary on the inner side of the subfield. To determine d and W, we first fit the subfields separately with a two-dimensional skew-normal distribution[49],

$$SN(x,y) = 2\phi(x,y) \times \Phi(x,y,\alpha_x,\alpha_y)$$

where φ is a two-dimensional Gaussian function and Φ is the two-dimensional integration of the Gaussian function. α_x and α_y are parameters regulating the shape of the distribution. When α_x and α_y equal 0, the function is a normal Gaussian. The fitting was performed to the raw data. The outlines of subfields were drawn where the values of fitted distribution are threefold of s.d. of baseline activity.

The distance between the peaks of spike On and Off subfields was normalized to the mean width of the subfields along the axis determined by their peaks. The distance between the peaks of membrane potential subfields or between those of synaptic subfields was normalized to the mean full-width at half-maximum of the two subfields along the axis determined by their peaks. The subfield size for spike receptive fields, the full-width at half-maximum bandwidth of synaptic receptive fields and the percentage shift of spike subfield boundaries were averaged for On and Off subfield.

The Youden's index was used to identify the boundary that best separate SRF and ORF cells.

$$\text{Youden's index} = \text{sensitivity} + \text{specificity} - 1$$
$$\text{Sensitivity} = \text{Probability}(SRF \mid V_m \text{ normalized distance} > a)$$
$$\text{Specificity} = \text{Probability}(ORF \mid V_m \text{ normalized distance} < a)$$

We changed the value of a to obtain the maximum Youden's index. The corresponding a value was the criteria to split SRF and ORF cells.

Modeling. We built a simple neuron model with a neuron receiving four sets of synaptic inputs evoked by On/Off stimuli. The spatial tuning curves of excitatory and inhibitory On responses were obtained by averaging the tuning curves from all the recorded SRF cells. The Off tuning curves were obtained by flipping the On tuning curves horizontally. The peaks of the Eon and Eoff were separated by 8° (average separation in the recorded SRF cells) and the overlapped Ion and Ioff were located in the middle between the Eon and Eoff (**Fig. 6a**). The temporal profile of the evoked synaptic response was generated by fitting the average synaptic current of the cell #1 with an alpha function:

$$\text{For } t > \text{onset}, G = \frac{G_{\max}(t - onset)}{\tau} e^{\frac{-(t - onset - \tau)}{\tau}}$$

with τ being 63 ms for the excitatory response and 83 ms for the inhibitory response (**Fig. 6a**). The onset of the inhibitory current was set at 5 ms after that of the excitatory current. The peaks of the excitatory and inhibitory tuning curves were set at 0.1 and 0.14 nA, respectively. The peak amplitudes of the evoked synaptic currents for each spatial location were determined from the tuning curves.

The spike response to On or Off stimulus at each spatial location was derived from the modeled synaptic inputs, based on the integrate-and-fire model. Overlap indexes were calculated from the spatial tuning curves in a similar way as described above. For synaptic tuning curves, the boundary was set at 10% of maximum response. For spike tuning curves, the boundary was set at where the first spike occurred.

39. Wagor, E., Mangini, N.J. & Pearlman, A.L. Retinotopic organization of striate and extrastriate visual cortex in the mouse. *J. Comp. Neurol.* **193**, 187–202 (1980).
40. Moore, C.I. & Nelson, S.B. Spatio-temporal subthreshold receptive fields in the vibrissa representation of rat primary somatosensory cortex. *J. Neurophysiol.* **80**, 2882–2892 (1998).
41. Margrie, T.W., Brecht, M. & Sakmann, B. *In vivo*, low-resistance, whole-cell recordings from neurons in the anaesthetized and awake mammalian brain. *Pflugers Arch.* **444**, 491–498 (2002).
42. de la Cera, E.G., Rodríguez, G., Llorente, L., Schaeffel, F. & Marcos, S. Optical aberrations in the mouse eye. *Vision Res.* **46**, 2546–2553 (2006).
43. Green, D.G., Powers, M.K. & Banks, M.S. Depth of focus, eye size and visual acuity. *Vision Res.* **20**, 827–835 (1980).
44. Remtulla, S. & Hallett, P.E. A schematic eye for the mouse and comparisons with the rat. *Vision Res.* **25**, 21–31 (1985).
45. Jagadeesh, B., Wheat, H.S., Kontsevich, L.L., Tyler, C.W. & Ferster, D. Direction selectivity of synaptic potentials in simple cells of the cat visual cortex. *J. Neurophysiol.* **78**, 2772–2789 (1997).
46. Somers, D.C., Nelson, S.B. & Sur, M. An emergent model of orientation selectivity in cat visual cortical simple cells. *J. Neurosci.* **15**, 5448–5465 (1995).
47. Hines, M. NEURON—a program for simulation of nerve equations. in *Neural Systems: Analysis and Modeling* (ed. Eeckman, F.) 127–136 (Spring, New York, 1993).
48. Schiller, P.H., Finlay, B.L. & Volman, S.F. Quantitative studies of single-cell properties in monkey striate cortex. I. Spatiotemporal organization of receptive fields. *J. Neurophysiol.* **39**, 1288–1319 (1976).
49. Azzalini, A. & Capitanio, A. Statistical applications of the multivariate skew-normal distribution. *J. R. Stat. Soc. Series B Stat. Methodol.* **61**, 579–602 (1999).

doi:10.1038/nn.2443